Revista Mexicana de Física **42**, *No. 2 (1996) 294–312*

Photonuclear reactions in ^{12}C and ^{28}Si

A. GÓMEZ*, E. MARTÍNEZ-QUIROZ
Instituto Nacional de Investigaciones Nucleares, Departamento del Acelerador
Apartado postal 18–1027, 11801 México, D.F., México

AND

T. UDAGAWA
Department of Physics, University of Texas at Austin
Austin, TX 78712, USA

Recibido el 5 de junio de 1995; aceptado el 17 de noviembre de 1995

ABSTRACT. The giant dipole resonance in ^{12}C and ^{28}Si is studied in the frame of the continuum random-phase-approximation theory. The behaviour of the resonance is analized for a momentum dependent particle-hole interaction of the Skyrme form. The predictions of the theory for the total photonuclear cross section and other photonuclear processes using different parametrizations of the p–h interaction are studied and the experimental data are compared with the calculations performed with the Skyrme-parametrization that best fits them.

RESUMEN. La resonancia dipolar gigante en ^{12}C y ^{28}Si es estudiada dentro de la aproximación de fases aleatorias. El comportamiento de la resonancia es analizada usando una interacción efectiva dependiente del momento del tipo de Skyrme. Las predicciones del método aquí presentado para la sección eficaz total y para otros procesos fotonucleares, mediante el uso de varias parametrizaciones de la interacción efectiva, son comparadas con los datos experimentales.

PACS: 25.20.Gf; 21.10.Re; 25.30.Cz

1. INTRODUCTION

The experimental data of photonuclear cross sections on doubly closed-shell nuclei show a complicated structure. The giant dipole resonance is normally observed as composed of a series of peaks whose varying strength gives the general shape of the resonance. Many theoretical efforts have been proposed to reproduce up to some degree this structure. Most of these efforts are limited to shell-model configurations with at most one nucleon in the continuum. These calculations yield cross sections whose structure is much simpler than the experimental one. As it has been shown by Gillet *et al.* [1], most of the observed experimental structure can be reproduced if more complicated configurations like 2p–2h are included.

In the present paper, we study the dipole photonuclear giant resonance for the slightly deformed nuclei ^{12}C and ^{28}Si, in the 1p–1h approximation. We make use of the coupled-channel continuum random phase approximation approach, which seems to be the most

* Correspondence to Dr. A. Gómez: Instituto Nacional de Investigaciones Nucleares, Departamento del Acelerador, apartado postal 18–1027, 11801, México D.F., México.

appropriate in the 1p–1h model. The basic purpose is to investigate the predictions of the theory for these nuclei using a velocity dependent p–h interaction and to find out how much of the experimental structure can be reproduced in the 1p–1h approximation.

It is true that we can not hope to reproduce the details of the structure of the dipole resonance. However, at least the gross structure will be predicted. It is also true that the nuclei ^{12}C and ^{28}Si are slightly deformed, nevertheless we think that a 1p–1h calculation in a spherical basis is meaningful from a semiquantitative point of view.

A new method has been proposed by Udagawa and Kim [2] to calculate the nuclear response in the continuum. In this theoretical approach the strength function is calculated within the frame of the continuum-random phase approximation. In this approach a very efficient method has been introduced to solve the inhomogeneous coupled-channel (CC) integro-differential equations obtained for particles excited by an external force. The large number and complexity of the CC-equations has been handled by modifying the basic equations and applying the Lanczos method to solve them. The advantages of this continuum RPA theory over others [3–5] lie mainly in the following points:

a) From a computational point of view, it is very efficient. That is, calculations for resonances of different multipolarity and for different nuclei, including heavy ones is executed in a matter of seconds. This is due primarily to the manner in which the CC-channel inhomogeneous equations obtained are modified and to the use of the Lanczos method to solve them [6]. The flexibility of our RPA has been proved by the calculations made for several nuclei ranging from light-medium nuclei such as the electric dipole resonance on ^{4}He, ^{16}O and ^{40}Ca [7], to heavy nuclei such as calculations for the monopole and quadrupole excitation modes on ^{90}Zr and ^{208}Pb [8].

b) The theory calculates simultaneously the p–h contributions to both, the direct emission and decay components of the total strength. This makes it possible to study several photonuclear processes, such as total photonuclear cross section (γ, N) and its components (γ, p) and (γ, n). The contributions coming from direct emission and damping effects can be predicted. Partial reactions like (γ, p_0), (γ, n_0), (γ, p_1), (γ, n_1), etc., can be equally calculated on the same footing.

In this work, we apply our continuum random phase approximation method to the study of the electric dipole resonance in some slightly deformed nuclei. In particular, we have focused our attention to the nuclei ^{12}C and ^{28}Si which from a theoretical point of view are interesting to study for the following points:

a) The experimental results for the excitation function of several photonuclear processes exhibit a complicated peak structure in the region of the resonance. As it is well known, most of this structure can be reproduced in a 2p–2h or 3p–3h calculations [1, 9], however it is important to see how much of this structure can be reproduced in a 1p–1h approximation. For this purpose we have used a momentum dependent p–h interaction. It has been shown that some of the structure can be reproduced with this kind of effective interaction for some spherical nuclei [10]. Therefore, it is our point to see if we can reproduce the main peak structure that the data show for the dipole resonance for the nuclei ^{12}C and ^{28}Si in our RPA method.

b) It has been argued from both an experimental and theoretical basis that the ground state of ^{28}Si contains a considerable admixture (> 30%) of more complicated states. Continuum calculations of the cross section of the $f_{7/2}$-reaction channel resulting from 1p–1h configurations greatly exceed the measured values as it has been shown by the calculation of Marangoni *et al.* [3]. The experimental integrated (γ, p_0) cross section up to a γ-ray energy of 25 MeV amounts to 21% of the giant electric photoabsorption cross section which is much smaller than the calculated 41%. In our calculation with the inclusion of a absorption potential to the excited particle states, we expect to reduce this overprediction.

A complete theoretical description of our continuum RPA formalism has been given elsewhere [2,7], here only a very brief description of the model will be presented. Emphasis will be given instead to the application to the nuclei considered.

Section 2 is dedicated to a brief mathematical description of our RPA model. Sections 3 and 4 are devoted to the application of the continunm RPA to calculations in the nuclei ^{12}C and ^{28}Si. Total photonuclear cross sections (γ, N) will be calculated and compared to experimental results. Partial components such as (γ, p) and (γ, n) will also be calculated. Photoemission processes like (γ, p_0), (γ, n_0), (γ, p_1) and (γ, n_1) will be predicted and whenever possible, comparison to experimental data will be made. Finally in Sect. 5, a discussion of the results and final conclusions are given.

2. Brief theoretical description

The electromagnetic dipole resonance is generally produced by the dipole component of the external electromagnetic field,

$$\hat{\rho} = \int d\mathbf{r}\, \Psi^+(\mathbf{r})\, \rho(\mathbf{r})\, \Psi(\mathbf{r}) \tag{1}$$

Ψ^+ and Ψ are field creation and annihilation operators given by

$$\Psi^+(\mathbf{r}) = \sum_{\mathrm{p}} \phi_{\mathrm{p}}(\mathbf{r})\, a_{\mathrm{p}}^+ \quad \text{and} \quad \Psi(\mathbf{r}) = \sum_{\mathrm{h}} \phi_{\mathrm{h}}(\mathbf{r})\, a_{\mathrm{h}}, \tag{2}$$

where $\rho(\mathbf{r}) = \sum_\mu e_{\mathrm{eff}} r Y_{1\mu}(\hat{r})$ is the dipole component of the electromagnetic field, ϕ_{p} and ϕ_{h} are single-particle and hole wave functions, $\hat{\rho}$ acting on the ground state of the target nucleus gives a superposition of 1p–1h states.

The total Hamiltonian for the 1p–1h states is considered as,

$$H = H_{\mathrm{h}} + H_{\mathrm{p}} + V_{\mathrm{ph}}, \tag{3}$$

where H_{h} is the hole-nucleus Hamiltonian, $H_{\mathrm{p}} = T_{\mathrm{p}} + U_{\mathrm{p}}$ is the excited particle Hamiltonian, consisting of the kinetic energy T_{p} and the complex optical potential U_{p}. V_{ph} is the p–h interaction which is assumed to be a local two-body interaction.

A hole-state ϕ_h of the core-nucleus with $(A-1)$ particles is given in terms of the quantum numbers of the missing particle.

The particle Hamiltonian H_p includes an imaginary potential $U_p = V_p + iW_p$, where the absorptive potential W_p is introduced to account for more complicated configurations (other than 1p–1h), not directly considered in the formalism.

We have not attempted to determine our potentials in a selfconsistent way, instead the Hartree-Fock potentials are sustituted by phenomenological average Woods-Saxon potentials whose parameters are determined by fitting the experimentally known particle- and hole-single particle energies. It is important to notice that ϕ_h as well as ϕ_p are eigenfunctions of different Hamiltonians, namely H_h and H_p, respectively. Also notice that ϕ_h represents the state of the core nucleus where only one particle is lacking.

In our continuum RPA calculations the important quantity is the strength function given by,

$$S = \frac{1}{\pi} I_m \left[- \int d\mathbf{r}\, d\mathbf{r}'\, \rho^*(\mathbf{r}) R(\mathbf{r}, \mathbf{r}'; E) \rho(\mathbf{r}') \right], \tag{4}$$

where the response function is defined as

$$R(\mathbf{r}, \mathbf{r}'; E) = \left\langle \phi_0 \middle| \Psi^+(\mathbf{r}) \hat{G} \Psi^+(\mathbf{r}') \Psi(\mathbf{r}') \middle| \phi_0 \right\rangle, \tag{5}$$

and $|\phi_0\rangle$ is the ground-state wave function. Further, $\hat{G}$ is the particle-hole Green's function of the target system,

$$\hat{G} = \frac{1}{E - H_h - H_p - V_{ph} + i\epsilon}, \tag{6}$$

where E is the excitation energy of the system. Using $\hat{G} = \hat{G}_0 + \hat{G}_0 V_{ph} \hat{G}$ where $\hat{G}_0 = 1/(E - H_h - H_p + i\epsilon)$ and introducing complete sets $\int d\mathbf{r}\, \Psi^+(\mathbf{r}) \Psi(\mathbf{r})$, then

$$R(\mathbf{r}, \mathbf{r}'; E) = R_0(\mathbf{r}, \mathbf{r}'; E) + \int d\mathbf{r}_1 d\mathbf{r}_1'\, R_0(\mathbf{r}, \mathbf{r}_1; E)\, V_{ph}(\mathbf{r}_1, \mathbf{r}_1')\, R(\mathbf{r}_1', \mathbf{r}'; E); \tag{7}$$

R_0 is the free response,

$$R_0(\mathbf{r}, \mathbf{r}'; E) = \left\langle \phi_0 \middle| \Psi^+(\mathbf{r}) \Psi(\mathbf{r}) \hat{G}_0 \Psi^+(\mathbf{r}') \middle| \phi_0 \right\rangle. \tag{8}$$

Introducing the function λ defined by means of

$$\int R(\mathbf{r}, \mathbf{r}'; E)\, \rho(\mathbf{r}')\, d\mathbf{r}' = \int R_0(\mathbf{r}, \mathbf{r}'; E)\, \lambda(\mathbf{r}')\, d\mathbf{r}', \tag{9}$$

then Eq. (7) can be written as

$$\lambda(\mathbf{r}) = \rho(\mathbf{r}) + \int d\mathbf{r}_1\, d\mathbf{r}_1'\, V(\mathbf{r}, \mathbf{r}_1)\, R_0(\mathbf{r}_1, \mathbf{r}_1'; E)\, \lambda(\mathbf{r}_1'), \tag{10}$$

therefore the strength function becomes

$$S = -\frac{1}{\pi} I_m \left[\int d\mathbf{r}\, d\mathbf{r}'\, \rho^*(\mathbf{r})\, R_0(\mathbf{r}, \mathbf{r}'; E)\, \lambda(\mathbf{r}') \right] \tag{11}$$

or more simply,

$$S = -\frac{1}{\pi} \mathrm{Im}\langle \rho | G_0 | \lambda \rangle. \tag{12}$$

As shown in Ref. [7], the strength function for a given p–h can be divided into two contributions:

$$S_{\mathrm{ph}} = S^{\uparrow}_{\mathrm{ph}} + S^{\downarrow}_{\mathrm{ph}}; \tag{13}$$

$S^{\uparrow}_{\mathrm{ph}}$ being the direct-emission part and $S^{\downarrow}_{\mathrm{ph}}$ the damping part given directly in terms of the absorptive potential W_{p} of the particle potential $U_{\mathrm{p}} = V_{\mathrm{p}} + iW_{\mathrm{p}}$. In fact,

$$S^{\downarrow}_{\mathrm{ph}} = -\langle \Psi | W_{\mathrm{p}} | \Psi \rangle, \tag{14}$$

with $|\Psi\rangle = \hat{G}_0 |\lambda\rangle$. The total emission and damping strengths are $S^{\uparrow} = \sum_{\mathrm{ph}} S^{\uparrow}_{\mathrm{ph}}$ and $S^{\downarrow} = \sum_{\mathrm{ph}} S^{\downarrow}_{\mathrm{ph}}$.

Finally the photoabsorption cross section can be calculated by

$$\sigma = \frac{8\pi^3(\lambda+1)}{\lambda[(2\lambda+1)!!]^2} k_\gamma^{2\lambda-1} S, \tag{15}$$

where $\lambda = 1$, for the dipole excitation. Clearly σ_{ph} as well as $\sigma^{\uparrow}_{\mathrm{ph}}$ and $\sigma^{\downarrow}_{\mathrm{ph}}$ can be calculated for a particular p–h configuration.

3. Application to ^{12}C and ^{28}Si

In this section, we apply our continuum RPA to the study the giant dipole resonance and other photonuclear process in ^{12}C and ^{28}Si. A Woods-Saxon potential will be used as an average Hartree-Fock potential for both; the particle-Hamiltonian H_{p} as well as for the hole-Hamiltonian H_{h}. The parameters of the average potential are determined so as to fit the experimental particle and hole single particle energies.

A momentum dependent interaction of the Skyrme form will be used for the interaction of the particle and core nucleus. Four different parametrizations of the p–h interaction will be used and final calculations will be performed with that parametrization that best fits the experimental peak and width of the dipole resonance.

We consider a Woods-Saxon optical potential which includes a spin-orbit term and a Coulomb repulsive part:

$$U(r) = -\frac{V_0}{1+f(r)} - \frac{iW_0}{1+f(r)} - \frac{4iW_0^s f(r)}{[1+f(r)]^2} + C(r)\delta_{\tau\frac{1}{2}} - V_0^s\left[\frac{\hbar}{m_\pi c}\right]^2 \frac{1}{ar}\frac{f(r)}{[1+f(r)]^2}\mathbf{l}\cdot\boldsymbol{\sigma}, \tag{16}$$

with $f(r) = \exp(r - R/a)$; the Coulomb term given by

$$C(r) = \begin{cases} \dfrac{Ze^2}{r}, & r \geq R; \\ \dfrac{Ze^2}{2R}\left[3 - \dfrac{r^2}{R^2}\right], & r < R. \end{cases}$$

Here $\hbar/m_\pi c$ is the Compton wavelength of the π–meson, $R = r_0(A-1)^{1/3}$ the radius of the residual nucleus. The imaginary potentials are applied only to the excited particle states to account for the effects of configurations more complicated than 1p–1h which are omitted in the 1p–1h model. In this calculation, we adopt the single-particle energies given by Endt and Van Der Leun [11]. The optical potential parameters that reproduce the experimental particle and hole(core-nucleus) single-particle energies are given in Table I. The residual particle-hole interaction to be used is a zero-range momentum dependent interaction of the Skyrme form, consisting of a two-body term

$$V(\mathbf{r}_1,\mathbf{r}_2) = t_0(1+x_0P_\sigma)\delta(\mathbf{r}_1-\mathbf{r}_2) + \tfrac{1}{2}t_1[\delta(\mathbf{r}_1-\mathbf{r}_2)\mathbf{k}^2 + \mathbf{k}'^2\delta(\mathbf{r}_1-\mathbf{r}_2)] + t_2\mathbf{k}\,\delta(\mathbf{r}_1-\mathbf{r}_2)\cdot\mathbf{k}' + i\omega_0(\boldsymbol{\sigma}_1+\boldsymbol{\sigma}_2)\cdot\mathbf{k}\times\delta(\mathbf{r}_1-\mathbf{r}_2)\mathbf{k}', \tag{17}$$

and a three-body term

$$V(\mathbf{r}_1,\mathbf{r}_2,\mathbf{r}_3) = t_3\delta(\mathbf{r}_1-\mathbf{r}_2)\delta(\mathbf{r}_2-\mathbf{r}_3).$$

The parametrizations of the interaction to be used in this work are shown in Table II.

3.1. ^{12}C results

Figure 1 shows the results obtained for the total photonuclear cross section $\sigma(\gamma, N)$ (Eq. (15)) for ^{12}C with the four parametrizations of the p–h interaction. As seen, the results obtained by using sky2 and sky3 parametrizations are very similar. They give the main resonance peak at about 20.7 MeV, while sky4 gives two main peaks shifted to lower energies, the strongest at 19.5 MeV. Only sky1 gives the correct position for the peak centered at 22.2 MeV which is very close to the observed position for the electric dipole resonance at 22.7 MeV. At this point, we apply a surface absorptive potential to the sky1 calculation of the form $W_0^s(\text{MeV}) = 0.05(E - E_f)$, E being the particle energy in the center

TABLE I. Single-particle energies and optical potential parameters for ^{12}C and ^{28}Si.

	protons						neutrons				
nlj	ϵ	V_0	V_{so}	a (fm)	r_0 (fm)	nlj	ϵ	V_0	V_{so}	a (fm)	r_0 (fm)
^{12}C											
$1s_{1/2}$	32.0	64.46	7.5	0.53	1.2	$1s_{1/2}$	35.1	63.96	7.5	0.53	1.2
$1p_{3/2}$	15.95	67.66	7.5	0.53	1.2	$1p_{3/2}$	18.71	67.12	7.5	0.53	1.2
$1p_{1/2}$	1.94	57.2	7.5	0.53	1.2	$1p_{1/2}$	4.95	60.8	7.5	0.53	1.2
$2s_{1/2}$	−0.42	57.0	7.5	0.53	1.2	$2s_{1/2}$	1.86	61.0	7.5	0.53	1.2
$1d_{5/2}$	−1.57	59.0	7.5	0.53	1.2	$1d_{5/2}$	1.1	62.0	7.5	0.53	1.2
$1d_{3/2}$	−6.28	57.0	7.5	0.53	1.2	$1d_{3/2}$	−3.39	60.0	7.5	0.53	1.2
^{28}Si											
$1s_{1/2}$	35.48	59.16	7.5	0.65	1.25	$1s_{1/2}$	43.90	61.08	7.5	0.65	1.25
$1p_{3/2}$	24.17	60.0	7.5	0.65	1.25	$1p_{3/2}$	28.41	57.92	7.5	0.65	1.25
$1p_{1/2}$	19.45	58.45	7.5	0.65	1.25	$1p_{1/2}$	22.3	54.09	7.5	0.65	1.25
$1d_{5/2}$	11.57	60.03	7.5	0.65	1.25	$1d_{5/2}$	17.21	59.97	7.5	0.65	1.25
$2s_{1/2}$	2.75	50.02	7.5	0.65	1.25	$2s_{1/2}$	8.5	54.0	7.5	0.65	1.25
$1d_{3/2}$	1.37	56.6	7.5	0.65	1.25	$1d_{3/2}$	7.2	56.0	7.5	0.65	1.25
$1f_{7/2}$	−1.03	58.0	7.5	0.65	1.25	$1f_{7/2}$	4.9	57.0	7.5	0.65	1.25
$2p_{3/2}$	−1.60	52.0	7.5	0.65	1.25	$2p_{3/2}$	3.6	54.0	7.5	0.65	1.25
$1f_{5/2}$	−7.0	56.0	7.5	0.65	1.25	$1f_{5/2}$	−1.3	58.0	7.5	0.65	1.25

TABLE II. Parameters of the Skyrme Interaction.

	t_0	t_1	t_2	t_3	X_0
sky I	−1057.3	235.9	−100.0	14463.5	0.56
sky II	−1169.9	586.6	−27.1	9331.1	0.34
sky III	−1128.75	395.0	−92.0	14000.0	0.45
sky IV	−1205.6	765.0	35.0	5000.0	0.05

of mass system and E_f the Fermi energy for emission, Fig. 2 shows this calculation up to an energy of 80 MeV compared to the data of Ahrens *et al.* [12] As seen the excitation function strength is very well predicted, the peak position has a small shift of 0.5 MeV to lower energies and the theoretical width is 5.3 MeV, 0.8 MeV larger than the recently experimental data of 4.5 MeV of Ref. [13]. For energies bigger than 35 MeV the decay of the cross section coincides excellently well with that observed. The peak at 17.4 MeV corresponds to proton emission from the $d_{5/2}p_{3/2}^{-1}$ configuration.

The calculated contributions (γ, n) and (γ, p) are shown in Figs. 3 and 4 compared to the data of Berman and Fultz [14] and of Ahrens *et al.* [12], respectively. The calculated

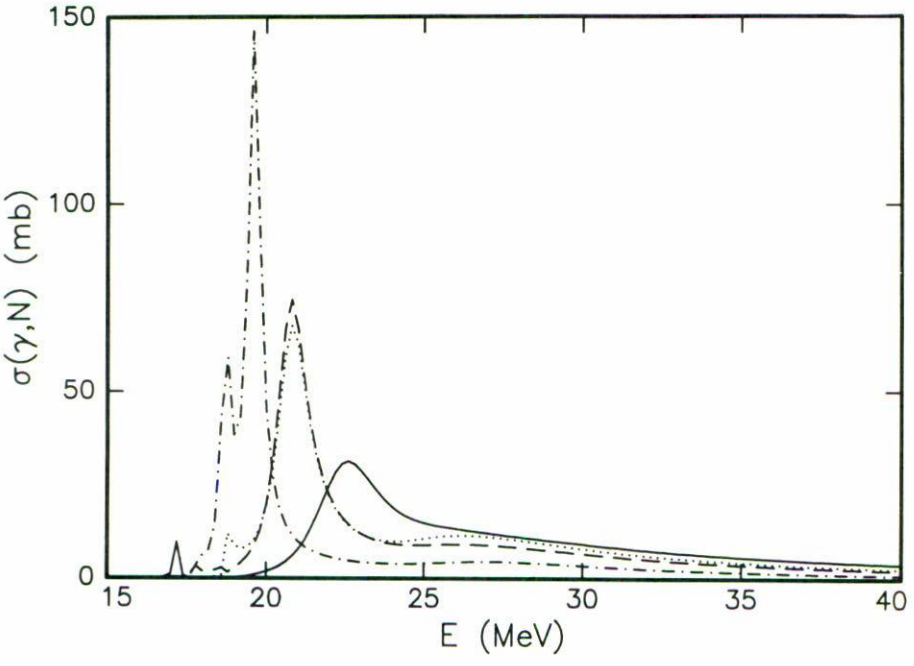

FIGURE 1. Total photoabsorption cross section for ^{12}C with a p–h interaction of the Skyrme form, where absorption potentials have not been applied. The solid line represents our calculation with the sky1 parametrization, the dotted line with the sky3, the dashed line with sky2, and the dotted-dashed line with the sky4 parametrization.

(γ, n) cross section gives well the position of the resonance, however at the peak, the magnitude is slightly overpredicted by about 1 mb and the width is 1.1 MeV larger. The corresponding (γ, p) calculation decays more slowly than the observed values, although the width is very well predicted.

We now turn our attention to the energy integrated cross section. In Fig. 5, we show the calculation obtained with our model for the energy integrated total photonuclear cross section compared to the corresponding experimental data [3]. Evidently our curve grows faster than the experimental points, this is due to the fact that the p–h interaction is velocity dependent as it will be discussed in the next section. Figure 6 shows the energy integrated (γ, N) and its (γ, p) and (γ, n) contributions, and Fig. 7 shows the contributions to the total energy integrated (γ, N) cross section from pure emission $\sigma^{\uparrow}$ [7].

3.2. ^{28}Si results

The experimental proton single particle and hole energies of Ref. [6] and neutron energies of Ref. [15] are fitted by using the Woods-Saxon potential parameters shown in Table I. The total photonuclear excitation function calculated up to 50 MeV with sky2 and sky3 parametrizations of the p–h interaction is shown in Figs. 8a and 8b, respectively. The corresponding experimental data are of Ahrens *et al.* [12] and an absorptive potential W_0^s as determined by Mahaux [16] has been applied. Figures 8c and 8d show the same calculation for the sky1 and sky4 parametrizations. The calculation with sky1 and sky4

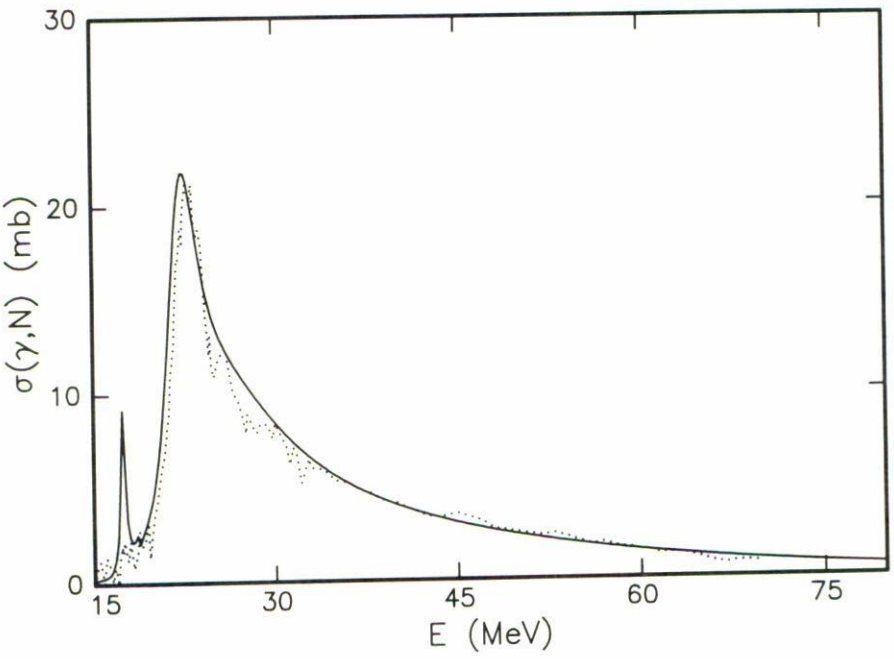

FIGURE 2. Total cross section for ^{12}C calculated with the sky1 parametrization compared with the data of Ahrens *et al.* [12]. In this calculation surface absoption potential W_0^s has been used.

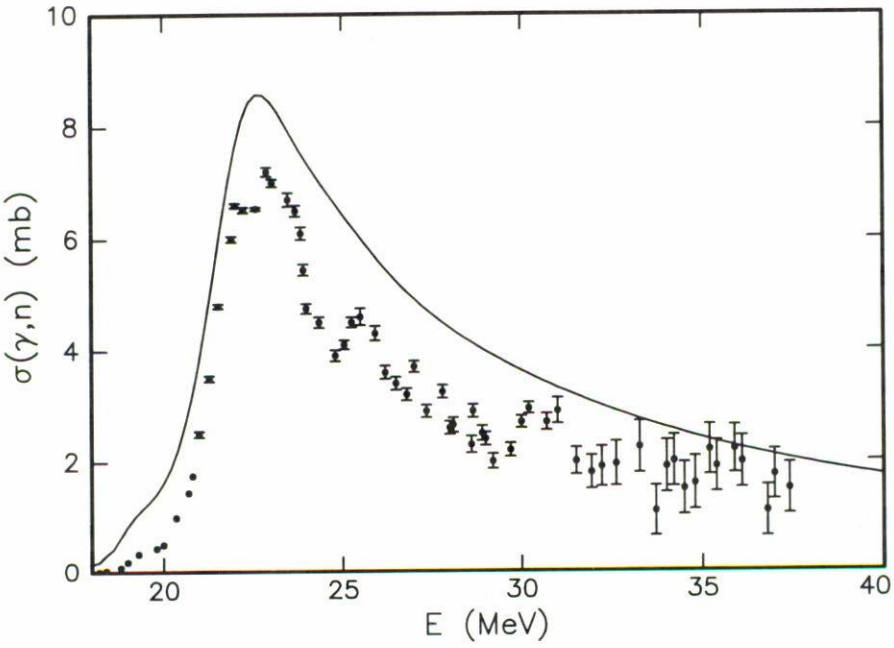

FIGURE 3. (γ, n) cross section for ^{12}C obtained with the sky1 parametrization of the Skyrme interaction compared to the experimental data of Ref. [14].

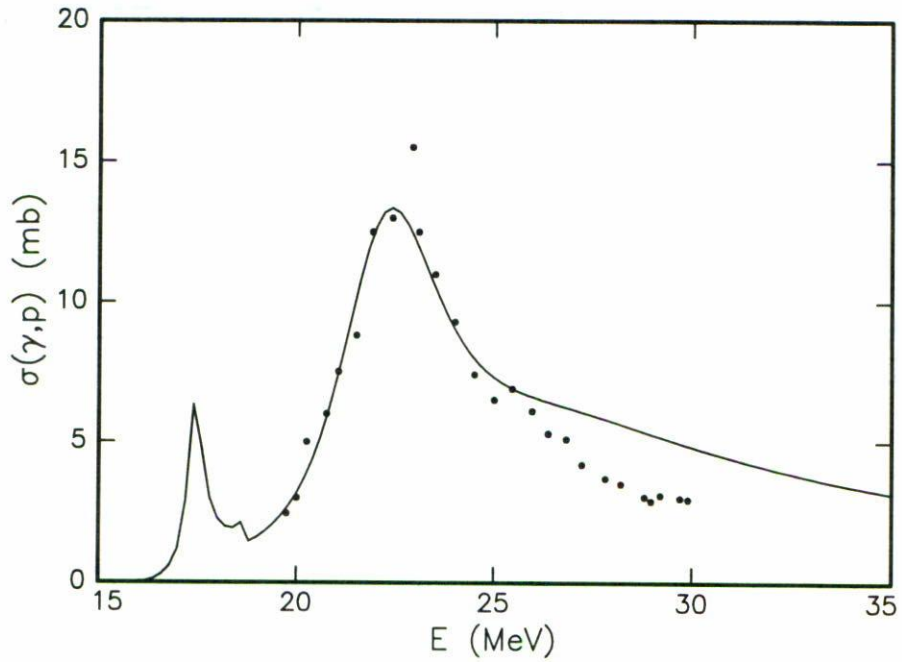

FIGURE 4. (γ, p) cross section for ^{12}C calculated with the sky1 parametrization, the data have been taken from Ref. [12].

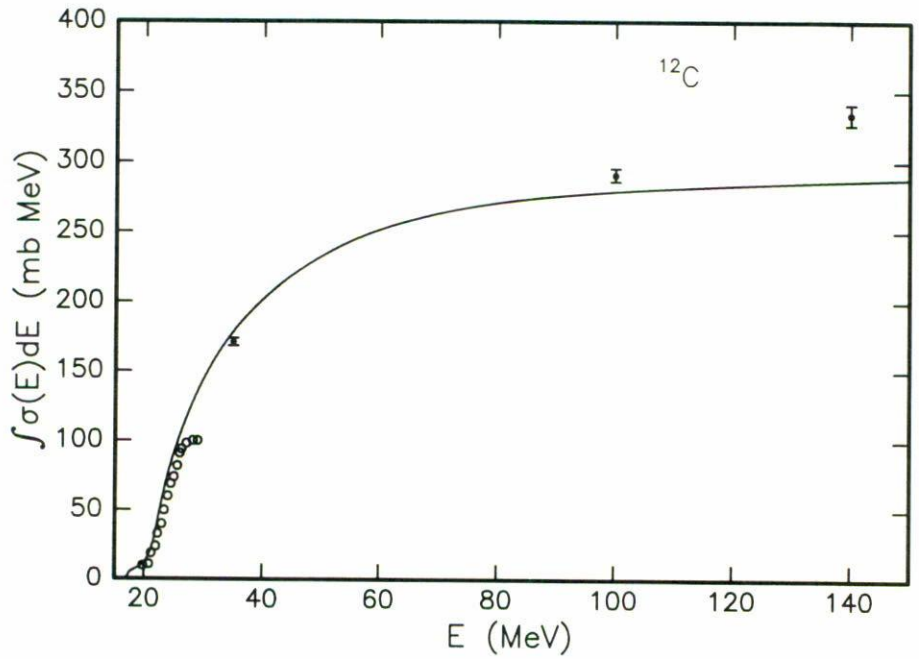

FIGURE 5. Integrated photonuclear cross section for ^{12}C using the sky1 parametrization, the experimental data correspond to Ref. [3].

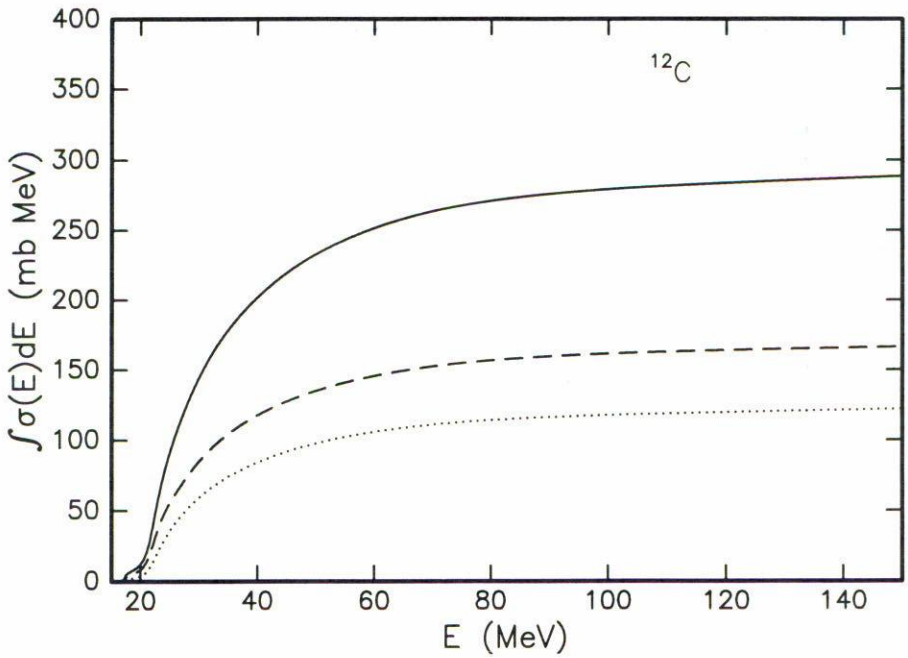

FIGURE 6. (γ, p) (dashed line) and (γ, n) (dotted line) contributions to the total integrated cross section (solid line). The calculation has been obtained with the sky1 parametrization.

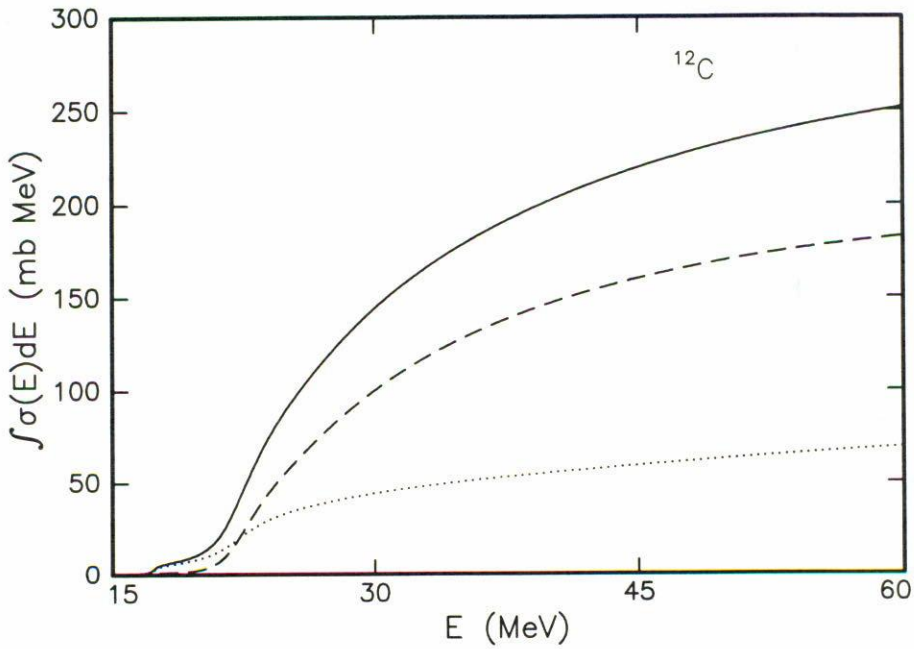

FIGURE 7. Direct emission $\sigma^{\uparrow}$ (dashed line) and spreading $\sigma^{\downarrow}$ (dotted line) contributions to the total integrated cross section. The sky1 parametrization has been used.

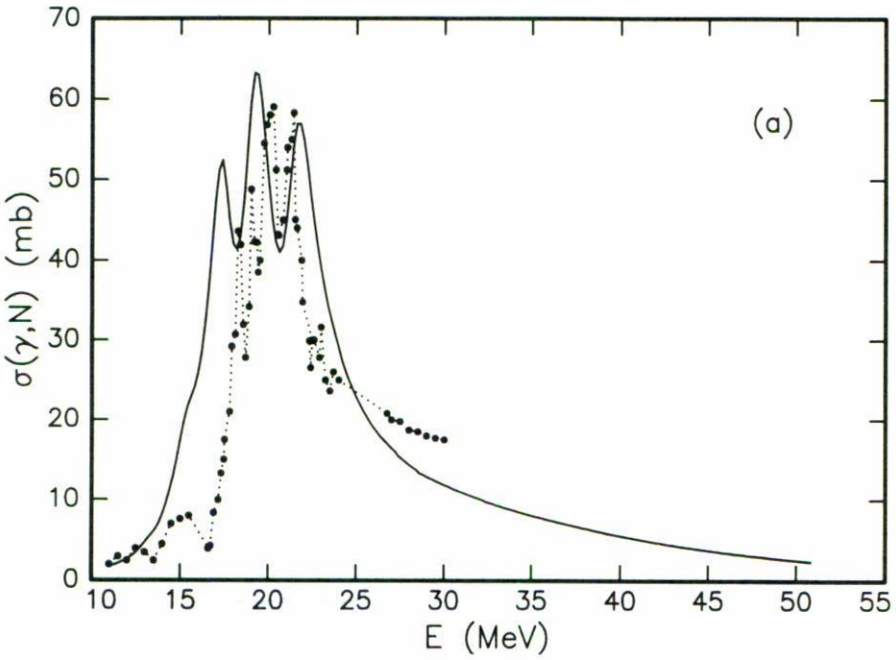

FIGURE 8. a) Total photonuclear cross section for ^{28}Si using the sky2 parametrization of the Skyrme interaction. The experimental data are taken from Ref. [12].

give a concentration of strength centered at energies around 21.5 MeV and 16.2 MeV, respectively, which are too far from the expected at 19.8 MeV, however the corresponding calculations with sky2 and sky3 are centered at 19.7 MeV and 20.6 MeV which are very close to the expected result. Clearly all the calculations overpredict the experimental resonance width.

With regard to the integrated photoabsorption cross section. The large values obtained for the decay width will necessarilly give large values for the integrated cross section. This is in part due to the momentum-dependent p–h interaction used in our calculations since, it is expected that such an interaction will conduct to results over the Thomas-Reiche-Khun (T-R-K) classical limit [17]. In Fig. 9, we show our calculations compared to the data of Ref. [18]. The calculations with sky1 and sky3 give closer results, although the sky2 and sky4 saturate faster.

The calculated (γ, p) cross sections for the sky2 and sky3 parametrizations are presented in Fig. 10, the experimental data are taken from Ref. [19] and finally the (γ, p) cross section for the sky2 calculation is shown in Fig. 11 together with its main p–h components.

4. DISCUSSION OF RESULTS AND CONCLUSIONS

Going back to Fig. 1 for the total photoabsorption cross section in ^{12}C, it can be seen that for this nucleus the Skyrme interaction has in general a very strong momentum-dependent component. This causes that the main peak of the dipole resonance be pushed to lower

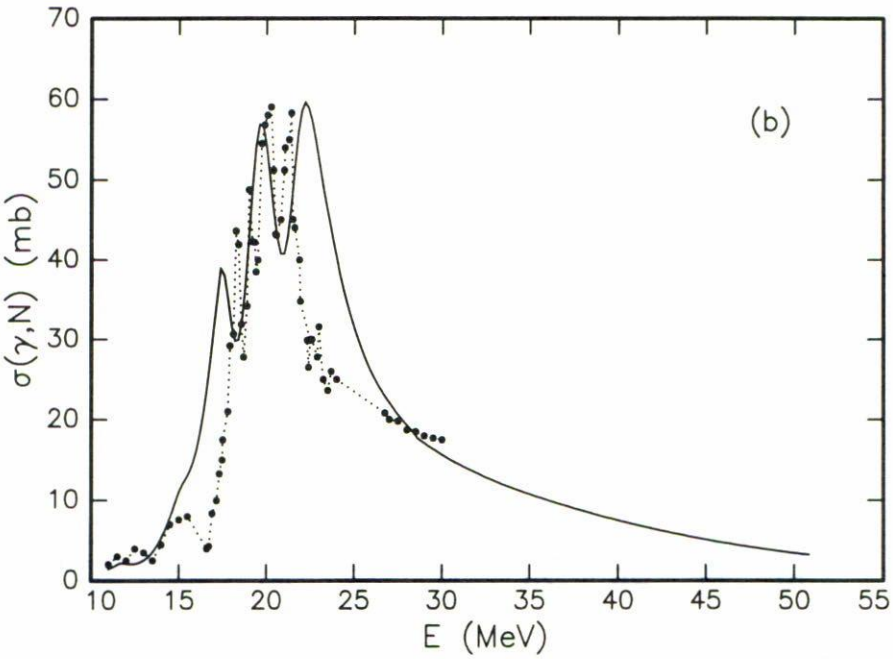

FIGURE 8. b) Total photonuclear cross section for ^{28}Si using the sky3 parametrization of the Skyrme interaction. The experimental data are taken from Ref. [12].

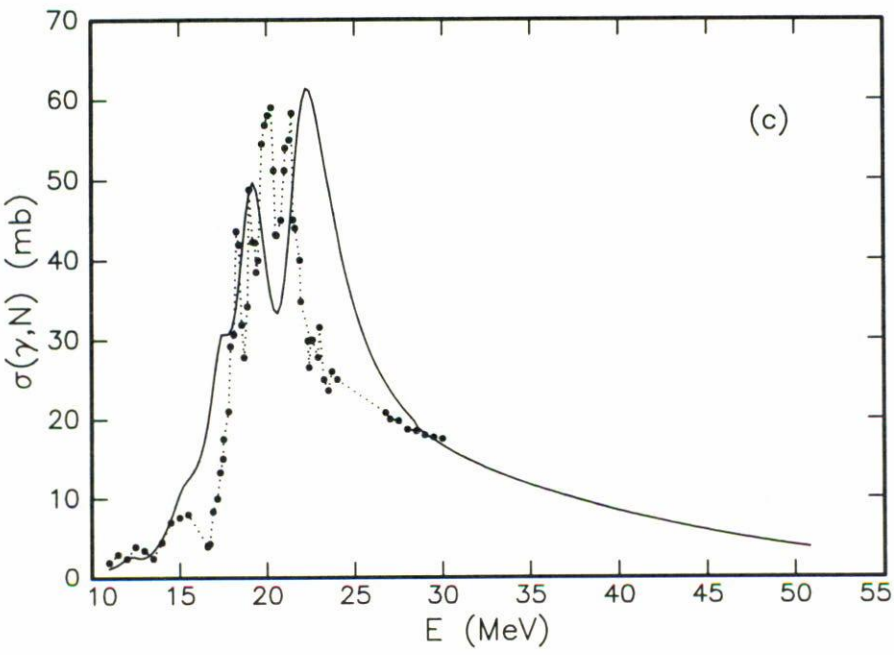

FIGURE 8. c) Total photonuclear cross section for ^{28}Si using the sky1 parametrization of the Skyrme interaction. The experimental data are taken from Ref. [12].

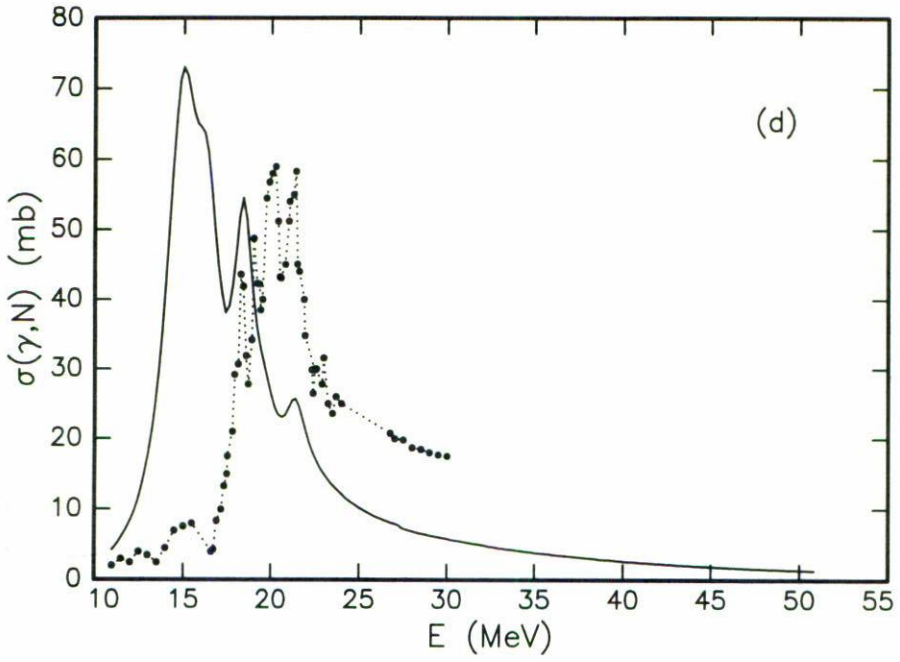

FIGURE 8. d) Total photonuclear cross section for ^{28}Si using the sky4 parametrization of the Skyrme interaction. The experimental data are taken from Ref. [12].

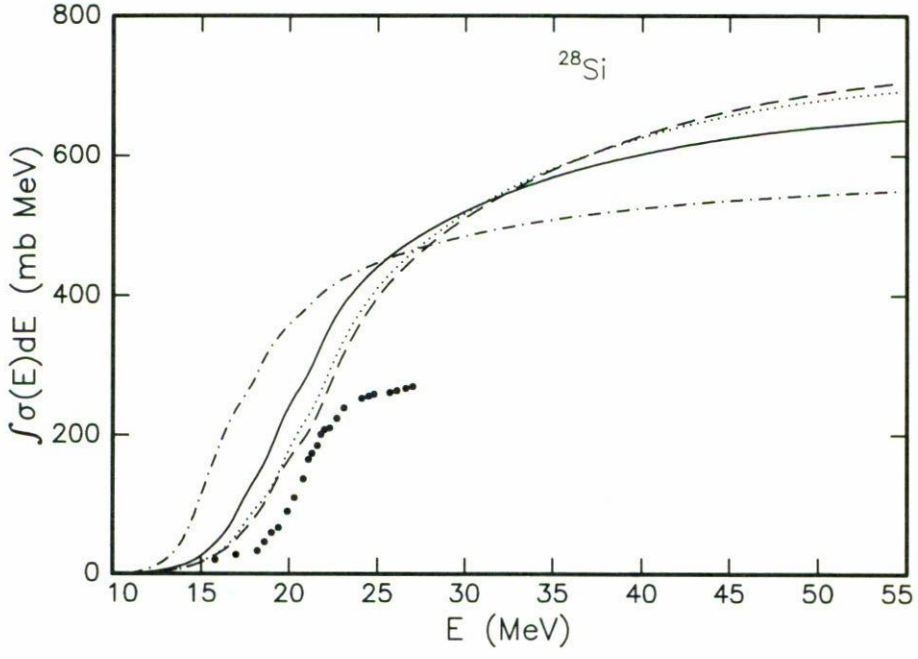

FIGURE 9. Total integrated cross section for ^{28}Si. The calculation with the sky1 parametrization corresponds to the dashed-line, the dotted line to sky3, the solid line to sky2 and the dotted-dashed line to sky4. The data are taken from Ref. [18].

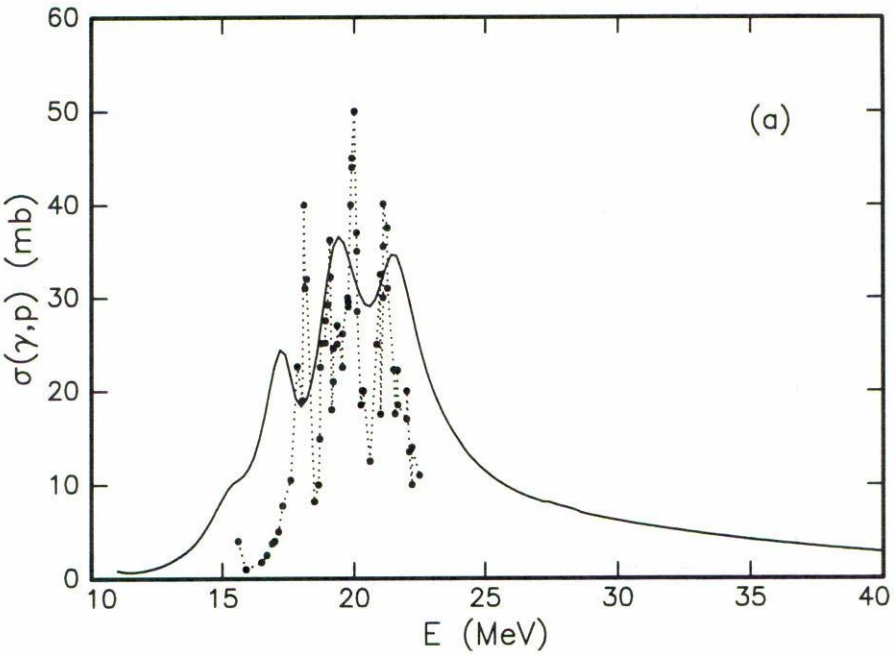

FIGURE 10. a) (γ, p) cross section (full line) obtained with the sky2 interaction compared to the data of Gulbranson *et al.* [19], the dotted line has been drawn to guide the eye.

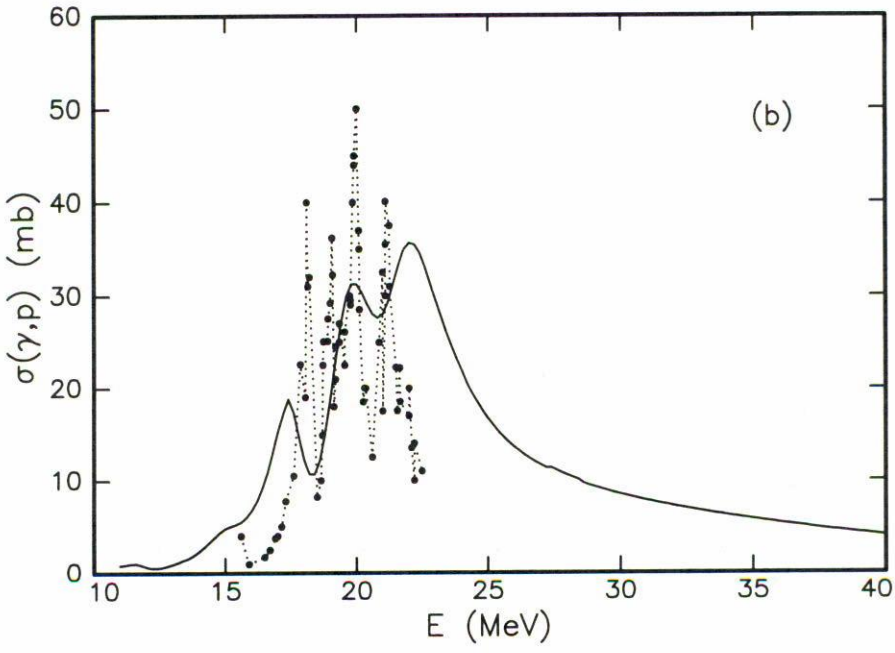

FIGURE 10. b) (γ, p) cross section (full line) obtained with the sky3 interaction compared to the data of Gulbranson *et al.* [19], the dotted line has been drawn to guide the eye.

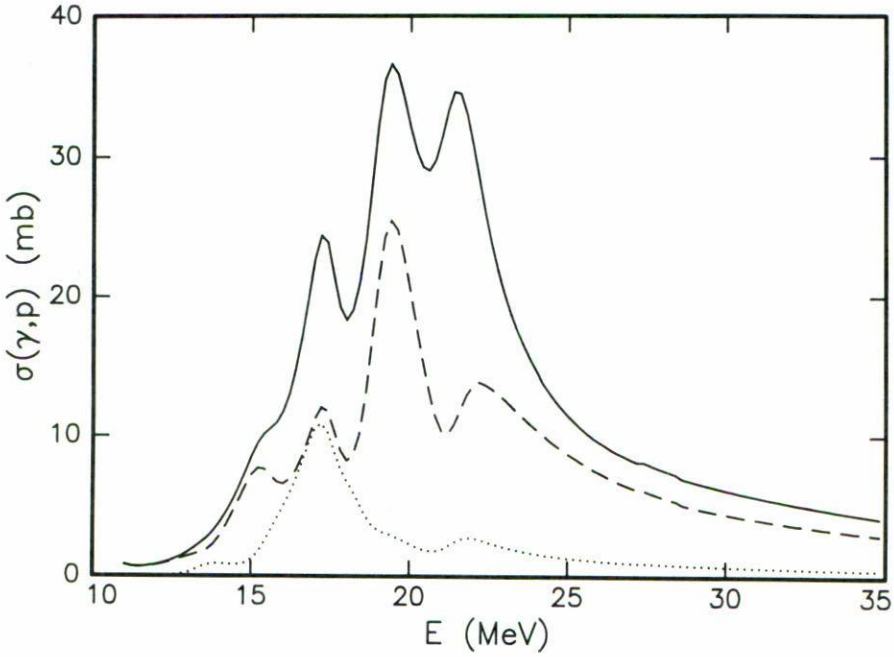

FIGURE 11. Main p–h contributions to the total (γ, p) cross section (full line), the dashed line corresponds to the transitions $f_{7/2}d_{5/2}^{-1}$, $f_{5/2}d_{5/2}^{-1}$ and $p_{3/2}d_{5/2}^{-1}$, while the dotted line includes the $s_{1/2}p_{1/2}^{-1}$ and $d_{3/2}p_{1/2}^{-1}$ transitions.

energies from the observed experimentally at 22.7 MeV. This momentum dependence is strongest for the sky4 parametrization and smaller in the sky1. Although the sky2 and sky3 parameters give very similar results, there is a slight shift of the sky2 interaction to lower energies. This behavior is not strange, it is well known that strong density dependent terms such as those in sky1 and sky3 have a repulsive effect while strong momentum dependent terms like sky2 and sky4, an attractive effect. The weak velocity dependence and strong density dependence of the sky1 interaction allows it to fit the expected resonance position. Figure 2 shows that by using the sky1 interaction, we have a excellent fit of the total cross section up to energies less than 70 MeV. The peak at 17.6 MeV corresponds to pure proton emission from the configuration $d_{5/2}p_{3/2}^{-1}$. The theoretical overprediction of the damping width (0.8 MeV) in the region of the giant resonance is a general consequence of the Skyrme interaction when used with absorptive potentials [7, 17]. An immediate effect of this overprediction is also evident in the integrated sum-rule shown in Fig. 5, where our calculated curve grows a little faster in the resonance region than the experimental data. It has been shown by Ring and Schuck [17] that a momentum dependent interaction without exchange mixtures does not obey the Thomas-Reiche-Kuhn sum rule classical limit,

$$\sigma_{\text{total}} = \int_0^\infty \sigma(E)\, dE \approx 60.0\, \frac{NZ}{A} \qquad \text{MeV-mb},$$

which for ^{12}C is 180 mb-MeV. Our calculation goes over that limit at 35.2 MeV and saturates at about 150 MeV with the limit of 290 mb-MeV. For higher energies our results

agree with the data of Mainz [12], for instance at 35, 100 and 140 MeV, we get for the integrated cross section 178.75, 279.24 and 287.01 mb-MeV, while the corresponding data at the same energies are 171, 291 and 342 mb-MeV respectively. The proton and neutron contributions to the total sum rule are 58.5% and 41.5% at 35 MeV, 57.7% and 42.13% at 100 MeV and 57.73% and 42.25% at 140 MeV respectively, in fact at 100 MeV, the ratio $\int dE\,\sigma(\gamma,p)/\int dE\,\sigma(\gamma,n)$ takes the value 1.373 diminishing very slowly for greater energies.

Another interesting point is the relative contribution to the total cross section from direct single particle emission and from damping into more complicated decay channels. As it was defined in Ref. [7], $\sigma^{\uparrow}$ refers to direct emission into the continuum from a hole orbit and depends on the real part of the particle potential $U_{\mathrm{p}} = V_{\mathrm{p}} + iW_{\mathrm{p}}$, while the spreading contribution $\sigma^{\downarrow}$ is proportional to the absorption strength $S^{\downarrow}$, *i.e.*,

$$\sigma^{\downarrow}(\gamma,N) = \frac{8\pi^3(\lambda+1)}{\lambda[(2\lambda+1)!!]^2}\, k_{\gamma}^{2\lambda-1}\, S^{\downarrow},$$

where λ is equal 1 for the dipole resonance, k^{λ} is the photon wavenumber and the total strengh is $S = S^{\uparrow} + S^{\downarrow}$, $S^{\uparrow}$ being its direct emission contribution.

Figure 7 shows that most of the cross section comes from direct particle emission, while the spreading into more complex configurations than 1p–1h increases slowly with the excitation energy. As a matter of fact the damping effect reaches its highest increase precisely at the peak of the resonance at 22.7 MeV where there is a high degree of collectivity.

As a general comment of our results, the overestimation of the damping widths in our calculations is a direct effect of the Skyrme interaction when used with absorptive potentials. As it has been pointed out by Cavignato *et al.* [10] a contrary effect occurs when a self-consistent calculation is applied, however it is clearly seen, that there will be an increase in the damping width if one tries to fit the strength of the resonance by the use of an absorptive potential. Recently new experimental data [20,21] reveal that there is evidence of an experimental underestimation in the contribution from the (γ,pn) channel, where the photon interacts a proton-neutron pair in the target nucleus, the proton is emitted while the neutron absorbs the recoil momentum, a more precise measurement of these effects is needed to verify the strength of the decay into this channel.

For the case of ^{28}Si, we have a similar behaviour of the Skyrme interaction. The sky2 and sky4 show a strong momentum term, therefore pushing the resonance to lower energies, while sky1 and sky3 to higher energies. The calculations with sky2 and sky3 parametrizations reproduce well the position of the main peak of the dipole resonance at 19.8 MeV, having a small shift of 0.1 MeV for the sky2 calculation and of 0.8 MeV for the corresponding sky3. The calculated width is of 7.5 MeV for sky2 and 7.9 MeV for sky2 and sky3 respectively. The measured data is 5.1 MeV [12], therefore there an overestimation of 2.4 MeV and 2.8 MeV for these calculations. Some of the basic resonance structure is obtained in our calculations, the sky2 gives three main peaks at 17.46, 19.4 and 22.1 MeV and the sky3 three peaks at 17.5, 20 and 22.6 MeV, while the experimental data show main peaks at 18.26, 19.0, 20.24 and 21.4 MeV. The main p–h components contributing to these peaks are $f_{7/2}d_{5/2}^{-1}$ for protons and $f_{7/2}d_{5/2}^{-1}$ and $s_{1/2}p_{3/2}^{-1}$ for neutrons.

Figure 9 shows again the characteristic behaviour of the Skyrme interaction. The increasing decay of the integrated dipole sum rule according to degree of influence of the momentum and density dependent terms of the parametrizations used. Therefore, sky4 decays faster, then sky2, finally sky3 and sky1. All four are above the T-R-K classical limit which for this case is 420 mb-MeV. Finally the main p–h transitions to the total (γ, p) are show in Fig. 11, clearly the $f_{7/2}d_{5/2}^{-1}$, $p_{3/2}d_{5/2}^{-1}$ and $f_{5/2}d_{5/2}^{-1}$ give the main contributions, especially at the peak at 19.8 MeV.

We may conclude our analysis by establishing the basic features found in our calculations. It is possible to use the Skyrme interaction in the study of the dipole resonance in light nuclei. There is a parametrization of the interaction that fits the experimental data of several photonuclear processes, either for ^{12}C (sky1) or ^{28}Si (sky2). The use of a momentum dependent p–h interaction with an absorptive potential leads in general to an overestimation of the decay width of excitation functions and of integrated sum rules. A systematics on the behaviour of excitation functions has also been established for the Skyrme interaction; sky1 and sky3 have a strong repulsive density dependence meanwhile sky2 and sky4 have strong attractive velocity dependence.

Clearly the main experimental resonance peak structure has been reproduced by our calculations for the two nuclei studied here, existing only small shifts from the expected peak positions. This shows again that a 1p–1h calculation is in some cases able to reproduce some of the basic structure of the giant resonance. The results of our calculations for the dipole resonance in the slightly deformed nuclei here presented show the effectiveness of our RPA method, the next step will be the application of our method to heavier and more deformed nuclei in a future work.

REFERENCES

1. V. Gillet, M.A. Melkanoff and J. Raynal, *Nucl. Phys.* **A97** (1967) 631.
2. T. Udagawa and B.T. Kim, *Phys. Rev.* **C40** (1989) 2271.
3. M. Marangoni and A.M. Sarius, *Nucl. Phys.* **A166** (1971) 397.
4. M. Marangoni, A. Sarius, *Nucl. Phys.* **A132** (1969) 649.
5. B. Buck and A.D. Hill, *Nucl. Phys.* **A95** (1967) 271.
6. A. Gómez and T. Udagawa, *Rev. Mex. Fís.* **38** (1992) 43.
7. A. Gómez and T. Udagawa, *Nucl. Phys.* **A565** (1993) 607.
8. T. Udagawa and B.T. Kim, *Phys. Lett.* **B230** (1990) 6.
9. A. Veyssiere, *Nucl. Phys.* **A159** (1970) 561.
10. M. Cavignato, M. Marangoni, P.L. Ottaviani and A.M. Sarius, *Nucl. Phys.* **A373** (1982) 445.
11. P.M. Endt and C. Van der Leun, *Nucl. Phys.* **A105** (1967) 1.
12. J. Ahrens, H. Borchert, K.H. Czock, H.B. Eppler, H. Gimm, H. Gundrum, M. Kröning, P. Riehn, G. Sita, A. Zieger and B. Ziegler, *Nucl. Phys.* **A251** (1975) 479.
13. S. Nakayama, T. Yamagata, M. Tanaka, M. Inoue, K. Yuasa, T. Itahashi, H. Ogata, N. Koori, K. Shima and M.B. Greenfield, *Phys. Rev.* **C 46** (1992) 1667.
14. B.L. Berman and S.C. Fultz, *Rev. of Mod. Phys.* (1975) 713.
15. S.A. Farris and J.M. Eisenberg, *Nucl. Phys.* **88** (1966) 241.
16. C.H. Johnson and C. Mahaux, *Phys. Rev.* **C 38** (1988) 2589.
17. P. Ring and P. Schuck, *The nuclear many-body problems*, Springer-Verlag, Berlin (1980) p. 294.
18. J.M. Wyckoff, B. Ziegler, H.W. Koch and R. Uhlig, *Phys. Rev.* **B 137** (1975) 576.

19. R.L. Gulbranson, L.S. Cardman, A. Doron, A. Erell, K.R. Lindgren and A.I. Yavin, *Phys. Rev.* **C 27** (1983) 470.
20. L. Van Hoorebeke, D. Ryckbosch, R. Van de Vyver, F. De Smet, J.O. Adler, B.E. Andersson, L. Isaksson, A. Sandell, B. Schröder and K. Ziakas, *Phys. Rev.* **C 45** (1992) 482.
21. D.A. Sims, S. Karataglidis, G.J. O'Keefe, R.P. Rassool, A.D. Bates, M.N. Thompson, S. Ito, H. Matsuyama, S. Sazaky, O. Koono and T. Terasawa, *Phys. Rev.* **C 45** (1992) 479.